J. Fluid Mech. (1980), *vol.* 99, *part* 1, *pp.* 33–52
Printed in Great Britain

Forward diffraction of Stokes waves by a thin wedge

By DICK K. P. YUE AND CHIANG C. MEI
R.M. Parsons Laboratory, Department of Civil Engineering,
Massachusetts Institute of Technology

(Received 18 May 1979 and in revised form 22 October 1979)

The diffraction of a steady Stokes wave train by a thin wedge with vertical walls is studied when the incident wave is directed along the wedge axis (grazing incidence). Parabolic approximation applied recently by Mei & Tuck (1980) to linear diffraction is extended to this nonlinear case. Significant effects of nonlinearity are found numerically, in particular the sharp forward bending of wave crests near the wedge. The computed features are found to corroborate the existing experiments only qualitatively; the controlling factors in the latter being not completely understood. An analytical model of stationary shock is proposed to approximate the numerical results of Mach stems.

1. Introduction

The diffraction of finite-amplitude waves in water is a matter of increasing practical importance in oceanographic engineering. Large structures for offshore exploration must be able to withstand the forces due to powerful storm waves. Breakwater entrances must also be designed for large waves. Current design practices are mostly based on model experiments in the laboratory and on theoretical estimates of the linearized theory. Theoretical developments of diffraction of finite-amplitude waves are so far scarce. For waves in water of intermediate or great depth, a second-order theory is available only for a two-dimensional floating body (Lee 1966). For three-dimensional motions the second-order theory for the simplest geometry of a vertical circular column was until recently (Molin 1979) controversial (Raman, Jothishankar & Venkatanarasaiah 1977; Isaacson 1977; Chakrabarti 1978). There exists very little experimental work which is relevant.

For long waves in shallow water, a very interesting phenomenon was found experimentally by Perroud (1957) and Chen (1961) and reported by Wiegel (1964*a*, *b*) for solitary waves incident obliquely on a straight wall. It is observed that, for angles of incidence less than 45°, the familiar linear picture that the incident and the reflected wave meet at the wall symmetrically about the normal to the wall, is replaced by a three-wave-crest system. In particular, there is now a third wave crest (called the *stem*) which intersects the wall normally; the incident wave and the stem meet at a point some distance away from the wall. For incidence angles less than 20° or so, the reflected crest disappears, leaving only the incident crest and the stem. Because of its geometrical resemblance to the reflexion of shock waves in gas dynamics (see Lighthill 1949; Whitham 1974) the phenomenon in shallow water waves has also been called *Mach reflexion* by Wiegel.

0022 1120/80/4462–1130 $02.00

Similar experiments of oblique incidence of periodic waves in finite water depth has been performed by Nielsen (1962) and more recently by Berger & Kohlhase (1976). The kinematics of the wave crests is much the same as in the case of solitary waves. From the experiments, the following features are noted. The wave amplitude along the barrier, i.e. the stem height, increases downwave for a finite distance and then levels off gradually. At any station, this amplitude increases with angle of incidence. The width of the stem region, which generally increases with distance along the wall, increases with decreasing incidence angle and with decreasing water depth. The stem width appears to be greater for longer incident waves. (This will be discussed later.) It is important to stress that there is substantial scatter in the experimental data, so that only general trends and qualitative conclusions can be made. In particular, the dependence on incident wave height is often ambiguous, although selected experiments indicate decreasing relative stem heights and increasing stem widths for higher waves. Aside from the usual concern for dissipation and errors in measurements, the scattering of data has been attributed to possible reflexions due to the finite length and width of the wave flume and diffraction from the far edge of the barrier, although the instability of Stokes waves may be another source of complication.

In shallow water a theory for the diffraction of solitary waves is now available by Miles (1977*a*, *b*) who applied Whitham's method of geometrical shock dynamics. For shallow water and linearized periodic waves at grazing incidence on a slender body, Mei & Tuck (1980) have recently found it expedient to employ the *parabolic approximation* first devised for radio-wave propagation over the earth by Leontovitch (1944) and Fock (1946, 1965) and now extended to many problems in acoustics (see Tappert 1977, and references therein). In this paper we further extend this approximation to nonlinear Stokes waves. It will be shown that the nonlinear diffraction of grazing incidence is governed by a cubic Schrödinger equation, a fact that can be anticipated in light of Mei & Tuck (1980). Numerical solutions are given for a vertical wedge with a small apex angle. All the computed results are in qualitative agreement with existing experiments, though precise comparison cannot be made until the scattering of experimental data is better understood. A simplified analytical model treating the region of Mach stems as one side of a shock is shown to agree surprisingly well with the computations. We have also obtained further numerical results for a grazing incidence of Stokes waves on a parabola and an island of finite length, and for the edge diffraction by a thin semi-infinite breakwater when the incidence is nearly normal. These results are much less dramatic and hence are not presented here.

Because of the side-band instability of Benjamin & Feir (1967) the time-dependent diffraction of transient Stokes waves (packets, trains) is likely to be even more important and interesting and will be the subject of a subsequent paper.

2. The parabolic approximation

We consider the diffraction of a plane Stokes wave (primary wavenumber k_0, amplitude A_0) from $x \sim -\infty$, by a thin long strut of width B, length L (along the x axis), and in water depth h.

It is assumed from the outset that the body is slender,

$$B/L \ll 1, \tag{2.1}$$

and long compared to the incoming wave,

$$k_0 L \gg 1. \tag{2.2}$$

Assuming inviscid, irrotational flow, the exact equations for the velocity potential ϕ and the free-surface elevation ζ are

$$\nabla^2\phi = 0 \quad \text{for} \quad -h < z < \zeta(x,y,t), \tag{2.3a}$$

$$g\phi_z + \phi_{tt} + |\nabla\phi|_t^2 + \tfrac{1}{2}(\nabla\phi.\nabla)|\nabla\phi|^2 = 0 \quad \text{on} \quad z = \zeta(x,y,t), \tag{2.3b}$$

$$\phi_z = 0 \quad \text{on} \quad z = -h, \tag{2.3c}$$

and

$$\phi_t + g\zeta + \tfrac{1}{2}|\nabla\phi|^2 = 0 \quad \text{on} \quad z = \zeta(x,y,t). \tag{2.3d}$$

The gravitational acceleration is designated by g.

2.1. *The approximate governing equation*

To fix ideas, let us recall the salient features of the linearized diffraction of short waves by a long body. Given vertical side walls for the entire sea depth, and linearizing (2.3), the velocity potential may be factorized as

$$\phi(x,y,z,t) = \Phi(x,y,t)\cosh k_0(z+h) \quad \text{for} \quad -h < z < 0, \tag{2.4}$$

and (2.3a) leads to the Helmholtz equation

$$\Phi_{xx} + \Phi_{yy} + k_0^2\Phi = 0 \quad \text{for} \quad -h < z < 0. \tag{2.5}$$

Since the longitudinal axis of the body is in the direction of wave propagation, and $k_0 L \gg 1$ and $B/L \ll 1$; we expect the backward scattering to be small so that the waves remain essentially propagating in the forward direction with the amplitude and phase modulated slowly in x (with the scale of L) and in y.

It is, therefore, reasonable to assume

$$\Phi = \mathrm{Re}\,(\Psi e^{ik_0 x}), \tag{2.6}$$

where

$$\Psi_x \ll k_0\Psi. \tag{2.7}$$

Substituting (2.6) into (2.5), we obtain

$$2ik_0\Psi_x + \Psi_{yy} + \Psi_{xx} = 0. \tag{2.8}$$

Clearly

$$2ik_0\Psi_x/\Psi_{xx} = O(k_0 L) \gg 1 \tag{2.9}$$

and the third term in (2.8) may be omitted with a relative error of $O(k_0 L)^{-1}$,

$$2ik_0\Psi_x + \Psi_{yy} = O(k_0 L)^{-1} k_0\Psi_x, \tag{2.10}$$

which implies that the length scale of transverse modulation L_y is given by

$$\frac{2ik_0}{L} \sim O\left(\frac{1}{L_y^2}\right) \quad \text{or} \quad \frac{L_y}{L} = O(k_0 L)^{-\frac{1}{2}}. \tag{2.11}$$

This is called the *parabolic approximation.*

Now, for Stokes wave, nonlinearity affects the wave at the leading order through the phase over a distance of $O(k_0\epsilon^2)^{-1}$, where ϵ is of the order of the wave slope. In order that nonlinear modulation and spatial modulation imposed by the body be equally important, we choose

$$(k_0\epsilon^2)^{-1} = O(L) \quad \text{or} \quad k_0 L = O(\epsilon^{-2}). \tag{2.12}$$

It follows from (2.11) that

$$k_0 L_y = O(\epsilon^{-1}). \tag{2.13}$$

Returning to the governing equations (2.3), we introduce the small ordering parameter ϵ and slow co-ordinates $X = \epsilon^2 x$ and $Y = \epsilon y$ as suggested by the preceding argument, and use multiple-scale expansions as follows:

$$\phi = \sum_{n=1} \epsilon^n \phi_n(x, X, Y, z, t) \tag{2.14}$$

and

$$\zeta = \sum_{n=1} \epsilon^n \zeta_n(x, X, Y, t) \tag{2.15}$$

with

$$\frac{\partial}{\partial x} \to \frac{\partial}{\partial x} + \epsilon^2 \frac{\partial}{\partial X}; \quad \frac{\partial}{\partial y} \to \epsilon \frac{\partial}{\partial Y}. \tag{2.16}$$

Details of the perturbation analysis are a mixture of Benney & Roskes (1969), Chu & Mei (1970) and Davey & Stewartson (1974), and an outline is given in the appendix for the sake of convenience. The result is as follows.

Let the first-order complex amplitude be A [see (A 11), (A 12)]; then the governing equation for A is

$$2\frac{\partial A}{\partial X} - \frac{i}{k_0}\frac{\partial^2 A}{\partial Y^2} + iK'|A|^2 A = 0, \tag{2.17}$$

where

$$K' = k_0^3 \frac{C_0}{C_{g0}} \frac{\cosh 4q + 8 - 2\tanh^2 q}{8\sinh^4 q}, \quad q \equiv k_0 h, \tag{2.18a}$$

$$C_0 = \omega/k_0 \tag{2.18b}$$

and

$$C_{g0} = \frac{\partial \omega}{\partial k_0} = \frac{\omega}{k_0 \sinh 2q}\left(\frac{\sinh 2q}{2} + q\right). \tag{2.18c}$$

Equation (2.17) is formally identical to the well-known cubic Schrödinger equation encountered in the study of unidirectional nonlinear evolution of dispersive waves (Zakharov & Shabat 1972), where X would take the role of time and Y the distance in the co-ordinate system travelling at group velocity. Although K' can take on different signs in general (Karpman 1975), in the present context it is always positive as defined by (2.18a), which corresponds to nonlinear dispersive waves without self-focusing or transverse side-band instability. We now turn to the boundary and initial conditions for (2.17).

2.2. *Boundary and initial conditions*

Let the body be symmetric about x axis and the walls be vertical throughout the sea depth and given by

$$y = \pm y_B(x), \quad \begin{cases} y_B = 0 & \text{for} \quad x \leqslant 0, \\ y_B \geqslant 0 & \text{for} \quad x > 0. \end{cases} \tag{2.19}$$

In the stretched co-ordinates, the body boundary is at

$$Y = \pm \epsilon k_0 B Y_B(X), \tag{2.20a}$$

where we have let

$$y_B = (k_0 B) Y_B \tag{2.20b}$$

with

$$k_0 Y_B = O(1). \tag{2.20c}$$

Considering the upper ($y > 0$) half of the symmetric problem, the boundary condition on the body is

$$\left.\begin{aligned} &\frac{D}{Dt}(y_B - y) = \phi_x y_{Bx} - \phi_y = 0 \quad (2.21a)\\ \text{or}\quad &\phi_y = \phi_x y_{Bx} \quad (2.21b)\end{aligned}\right\} \quad \text{on} \quad y = y_B.$$

Using (2.20), (2.21*b*) becomes in normalized variables

$$\epsilon\phi_Y = \left[\left(\frac{\partial}{\partial x} + \epsilon^2\frac{\partial}{\partial X}\right)\phi\right]\epsilon^2 k_0 B Y'_B(X) \quad \text{on} \quad Y = \epsilon k_0 B Y_B(X) \tag{2.22}$$

and, substituting in the expression for ϕ from (A 11), we obtain

$$\begin{aligned}\epsilon\Big[-\frac{g\cosh Q}{2\omega\cosh q}(iA_Y e^{i\psi} + *) + \phi_{01Y} + O(\epsilon)\Big] \\ = \left\{-\frac{g\cosh Q}{2\omega\cosh q}[i(ik_0 A^{i\psi} + *] + O(\epsilon)\right\}\epsilon^2(k_0 B)\, Y'_B(X) \quad \text{on} \quad Y = \epsilon k_0 B Y_B(X).\end{aligned} \tag{2.23}$$

We now equate the first harmonic terms in (2.23) so that, to leading order,

$$\frac{\partial A}{\partial Y} = ik_0 A \epsilon k_0 B Y'_B(X) \quad \text{on} \quad Y = \epsilon k_0 B Y_B(X). \tag{2.24}$$

We now have two possibilities for the body width compared to wavelength.

(i) Thin strut: $k_0 B = 1$, and (2.24) becomes

$$\partial A/\partial Y = \epsilon i k_0 A\, Y'_B(X) \quad \text{on} \quad Y = \epsilon Y_B, \tag{2.25}$$

so that the body only affects the waves at $O(\epsilon)$.

(ii) Moderately thin strut: $k_0 B = \epsilon^{-1}$. Note that, in this case, $B/L \sim O(\epsilon)$ and the body is still thin compared to length. The boundary condition (2.24) now affects A at the leading order and becomes

$$\partial A/\partial Y = ik_0 A\, Y'_B(X) \quad \text{on} \quad Y = Y_B(X), \tag{2.26}$$

which must be applied exactly on the body.

We shall henceforth concentrate on the moderately thin strut and consider (i) as only a special case of (ii).

Far away from the body, at large Y, we expect no transverse variations, and the boundary condition is

$$\partial A/\partial Y \to 0, \quad Y \to \infty, \tag{2.27a}$$

or using (2.17),

$$A \to A_0 e^{-\frac{1}{2}iK'A_0^2 X}, \quad Y \to \infty, \tag{2.27b}$$

which is simply the undisturbed uniform Stokes wave. The appropriate initial condition just ahead of the body is

$$A = A_0, \quad X = 0. \tag{2.28}$$

We further introduce the non-dimensional variables

$$\bar{A} = A/A_0, \quad \bar{X} = k_0 X = \epsilon^2 k_0 x, \quad \bar{Y} = k_0 Y = \epsilon k_0 y, \quad \bar{Y}_B = k_0 Y_B. \tag{2.29}$$

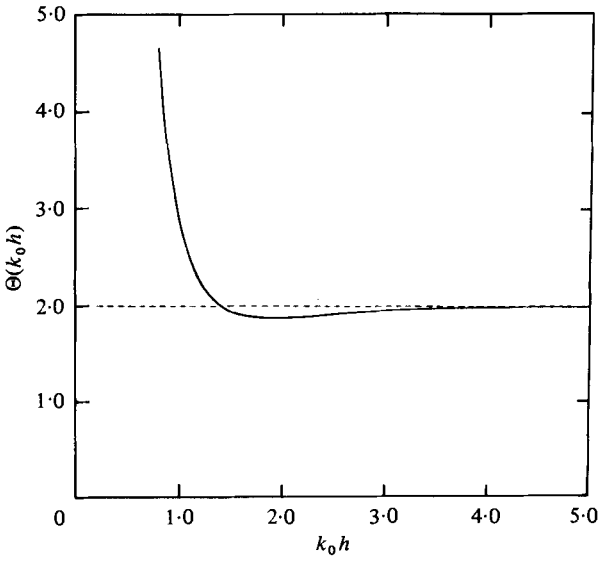

FIGURE 1. Plot of Θ *vs.* $k_0 h$.

The normalized initial boundary-value problem may be stated as follows:

$$2\frac{\partial \bar{A}}{\partial \bar{X}} - i\frac{\partial^2 \bar{A}}{\partial \bar{Y}^2} + iK|\bar{A}|^2\bar{A} = 0 \quad \text{for} \quad \bar{Y} > \bar{Y}_B(\bar{X}), \quad \bar{X} > 0, \tag{2.30a}$$

$$\bar{A} = 1, \quad \text{on} \quad \bar{X} = 0, \tag{2.30b}$$

$$\frac{\partial \bar{A}}{\partial \bar{Y}} = i\bar{Y}'_B(\bar{X})\bar{A}, \quad \text{on} \quad \bar{Y} = \bar{Y}_B(\bar{X}), \tag{2.30c}$$

$$\frac{\partial \bar{A}}{\partial \bar{Y}} \to 0 \quad \text{or} \quad \bar{A} \to e^{-\frac{1}{2}iK\bar{X}} \quad \text{as} \quad \bar{Y} \to \infty. \tag{2.30d}$$

The parameter K is now given by

$$K = (k_0 A_0/\epsilon)^2 \Theta(k_0 h) \tag{2.31}$$

with

$$\Theta(k_0 h) = \frac{C_0}{C_{g0}} \frac{\cosh 4k_0 h + 8 - 2\tanh^2 k_0 h}{8\sinh^4 k_0 h}. \tag{2.32}$$

Figure 1 is a plot of Θ against $k_0 h$. Note that Θ approaches 2 for $k_0 h \to \infty$ but grows as $(k_0 h)^{-4}$ for $k_0 h \to 0$ in shallow water.

Equation (2.30) must now be solved for the first-order wave envelope $\bar{A}(\bar{X}, \bar{Y})$.

2.3. *Method of numerical solution*

Since the boundary condition (2.30*c*) is applied on the body surface, analytic solution to the nonlinear equation is difficult and one must in general integrate (2.30*a*) numerically.

The numerical computation marches forward in $\bar{X}$. The range of $\bar{Y}$, $\bar{Y}_B(\bar{X}) < \bar{Y} < \bar{Y}_\infty$, is chosen to be sufficiently large so that further increase of $\bar{Y}_\infty$ produces no significant changes in the solution.

Equation (2.30*d*) is replaced by

$$\left.\begin{aligned}\partial\bar{A}/\partial\bar{Y} &= 0\\ \text{or}\qquad \bar{A} &= e^{-\frac{1}{2}iK\bar{X}}\end{aligned}\right\} \quad \text{on} \quad \bar{Y} = \bar{Y}_\infty. \tag{2.33a}$$

$$\tag{2.33b}$$

For (2.30*a*), we employ an implicit scheme of Crank–Nicholson type for integration in $\bar{X}$, and centred second-order differencing in $\bar{Y}$:

$$2\bar{A}_j^{n+1} = 2\bar{A}_j^n + \frac{\Delta\bar{X}}{2}\left[\left(i\frac{\bar{A}_{j+1}^{n+1} - 2\bar{A}_j^{n+1} + \bar{A}_{j-1}^{n+1}}{\Delta\bar{Y}^2} - iK|\bar{A}_j^{n+1}|^2\bar{A}_j^{n+1}\right)\right.$$
$$\left. + \left(i\frac{\bar{A}_{j+1}^n - 2\bar{A}_j^n + \bar{A}_{j-1}^n}{\Delta\bar{Y}^2} - iK|\bar{A}^n|^2\bar{A}^n\right)\right] + O(\Delta\bar{X}^3, \Delta\bar{Y}^2), \tag{2.34a}$$

where

$$2\bar{A}_j^{n+1} = 2\bar{A}_j^n + \Delta\bar{X}\left(i\frac{\bar{A}_{j+1}^n - 2\bar{A}_j^n + \bar{A}_{j-1}^n}{\Delta\bar{Y}^2} - iK|\bar{A}^n|^2\bar{A}^n\right) + O(\Delta\bar{X}^2, \Delta\bar{Y}^2), \tag{2.34b}$$

$$\bar{A}_j^n \cong \bar{A}(n\Delta\bar{X}, j\Delta\bar{Y}), \tag{2.34c}$$

$$n = 1, 2, \ldots, N, \tag{2.34d}$$

$$j = j_B^n + 1, j_B^n + 2, \ldots, J-1, \quad \begin{cases}\bar{Y}_B(n\Delta\bar{X}) = j_B^n\Delta\bar{Y},\\ \bar{Y}_\infty = J\Delta\bar{Y}.\end{cases} \tag{2.34e}$$

For $j = j_B^n$, (2.34*a*) is modified by boundary condition (2.30*c*),

$$\frac{\bar{A}_{j+1}^m - \bar{A}_{j-1}^m}{2\Delta\bar{Y}} = i\bar{Y}'_B(m\Delta\bar{X})\,\bar{A}_j^m + O(\Delta\bar{Y})^2, m = n, n+1 \tag{2.35}$$

and, of course, for $j = J$, (2.33*b*) gives

$$\bar{A}_J^m = e^{-\frac{1}{2}iKm\Delta\bar{X}}, \quad m = n, n+1. \tag{2.36}$$

Equation (2.34*a*), which has a global truncation error of $(\Delta\bar{X}^2, \Delta\bar{Y}^2)$, is well known to be unconditionally stable for the linear problem, and is found to be stable for reasonable choices of $\Delta\bar{X}$ and $\Delta\bar{Y}$ in the fully nonlinear case. From equation (2.30) a conservation law may be derived,

$$\frac{\partial}{\partial\bar{X}}\int_{\bar{Y}_B(\bar{X})}^{\infty}|\bar{A}|^2 d\bar{Y} = 0, \tag{2.37}$$

which reduces to

$$\int_{\bar{Y}_B(\bar{X})}^{\bar{Y}_\infty}|\bar{A}|^2 d\bar{Y} = \bar{Y}_\infty - \bar{Y}_B(0) = \bar{Y}_\infty \tag{2.38}$$

for a finite region. Equation (2.38) is used as a measure of the total error due to discretization, round-off, and truncation of $\bar{Y}_\infty$; and is satisfied to within a few per cent for all computed cases.

3. Numerical results for grazing incidence on a thin wedge

For a train of Stokes waves incident along the axis of a vertical wedge of small half-angle α (i.e. $y_B = x\tan\alpha$), we define the width-to-length ratio $\epsilon \equiv \tan\alpha$, so that

$$\bar{Y}_B(\bar{X}) = \bar{X} \tag{3.1}$$

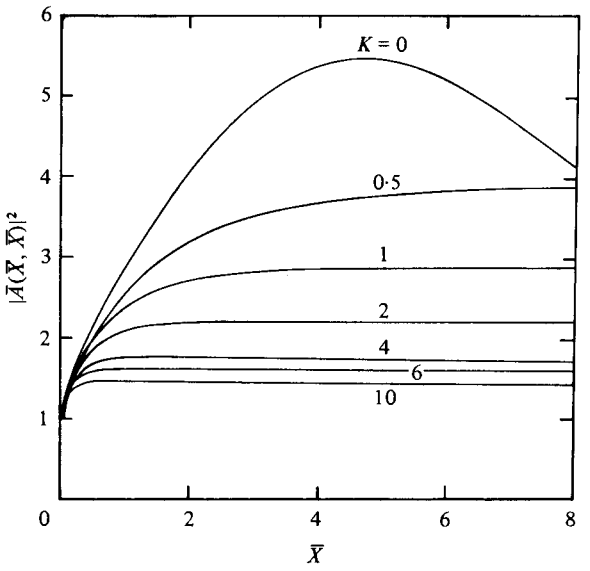

FIGURE 2. Magnitude squared of the envelope at the wall: $|\bar{A}(\bar{X}, \bar{Y} = \bar{X}; K)|^2$, for different values of K.

and equations (2.51a), (2.51c) become

$$2\frac{\partial \bar{A}}{\partial \bar{X}} - i\frac{\partial^2 \bar{A}}{\partial \bar{Y}^2} + iK|\bar{A}|^2\bar{A} = 0 \quad \text{for} \quad \bar{Y} > \bar{X} > 0, \tag{3.2a}$$

$$\frac{\partial \bar{A}}{\partial \bar{Y}} = i\bar{A} \qquad \text{on} \quad \bar{Y} = \bar{X}. \tag{3.2b}$$

The governing equations now contain a single parameter K given by (2.31), which depends only on the incident wave characteristics and the wedge angle. In particular, for deep water ($k_0 h \to \infty$)

$$K \sim 2(k_0 A_0/\epsilon)^2, \tag{3.3}$$

which is simply twice the square of the wave steepness relative to wedge thickness.

Equations (3.2), (2.30b) and (2.33b) are solved numerically for a range of K and for $0 < \bar{X} < 8$ and $Y_\infty = 100$.

Figure 2 shows a plot of $|\bar{A}|^2$ along the wedge (on $\bar{Y} = \bar{X}$) for the different K values. For $K = 0$ (the linear case), an analytic solution can be directly obtained, with

$$|A(\bar{X}, \bar{Y} = \bar{X})|^2 = |1 + \mathrm{erf}(-\tfrac{1}{2}i\bar{X})^{\frac{1}{2}}|^2, \tag{3.4}$$

which oscillates about 4 and approaches it as $1/\bar{X}$ for $\bar{X} \gg 1$. Equation (3.4) is indistinguishable from the computed $K = 0$ curve in figure 2. Note in figure 2 that, in contrast to the linear case, the amplitude along the wedge for $K > 0$ grows for a short distance, then flattens out to a constant value. This value decreases with increasing K and we define for further reference

$$E_-(K) = |\bar{A}(\bar{X} = 8, \bar{Y} = \bar{X}; K)|^2. \tag{3.5}$$

Noting the dependence of K on wave steepness and wedge slope, the qualitative features of figure 2 for the wave height along the wall are in agreement with earlier experimental observations.

K	0	0·5	1	2	4	6	10
$\beta(K)$	1·00	1·03	1·23	1·50	1·94	2·28	2·82

TABLE 1

For a global picture of the wave envelope, we display its magnitude squared, $|\bar{A}(\bar{X}, \bar{Y})|^2$ (which is also proportional to the second-order mean set-down), in three-dimensional plots for $K = 0, 2, 6$ (see figure 3 (a, b, c)), where the wedge is given a height of 5 (note that $|\bar{A}|^2 = 1$ at $\bar{X} = 0$) to provide a visual reference. The linear case ($K = 0$) is presented here for comparison.

For the nonlinear cases ($K > 0$), the overall amplitudes are much smaller than the linear case (decreasing as K increases), and there is a clearly defined region along the wall within which $|\bar{A}|^2$ has a nearly constant value ($\sim E_-(K)$). The width of this flat region appears to increase linearly with $\bar{X}$, at an angle which increases with K. Outside of this region, the envelope undulates in a way qualitatively similar to that observed for the linear case. A more quantitative picture of these features can be obtained by studying successive cross-sections of $|\bar{A}(\bar{X} = \bar{X}_i, \bar{Y})|^2$, and defining (rather arbitrarily) a width $\bar{Y} = M(\bar{X}; K)$ corresponding to the edge of the flat region. Figures 4 (a, b, c) show some examples for $K = 0$, 2, 6 at $\bar{X}_i = 4$ and 8. The increasing width with K and $\bar{X}$ is evident. We summarize the results for $M(\bar{X}, K)$ in figure 5, where the points are from the computed results, and the straight lines their least-square linear fit. We see that the linear correlations are excellent, suggesting an empirical relationship of the form

$$M(\bar{X}; K) = \beta(K)\,\bar{X}. \tag{3.6}$$

The values β for different K are shown in table 1. We shall return to the dependence $\beta(K)$ later.

For more physical information, we computed the first-order instantaneous free surface elevation

$$\zeta_1(k_0 x, k_0 y, t = 0) = \mathrm{Re}\{\bar{A}(\epsilon^2 k_0 x, \epsilon k_0 y)\, e^{ik_0 x}\}, \tag{3.7}$$

using the fact that $\bar{X} = \epsilon^2 k_0 x$ and $\bar{Y} = \epsilon k_0 y$. Note that, for the same k_0, the incoming Stokes wave has a longer wavelength for increasing nonlinearity given by the asymptotic behaviour $\bar{A} \to e^{-\frac{1}{2}iK\bar{X}}$ as $\bar{Y} \to \infty$. Here we display three-dimensional and contour plots of ζ_1, but this time in uniformly scaled $k_0 x$ and $k_0 y$ co-ordinates, so that all physical angles are undistorted (see figures 6 and 7). The parameter chosen is for $K = 0$, 1, 2, and for wedge slopes corresponding to $\epsilon^2 = 0{\cdot}1$ and $0{\cdot}15$ (half apex angles of $\alpha \simeq 17{\cdot}55°$ and $21{\cdot}17°$ respectively). We caution that these values of K and ϵ^2 are selected here to accentuate the important features, and may correspond to steeper waves than the theory permits. In particular, for the steepest case presented: $K = 2$, $\epsilon^2 = 0{\cdot}15$, the wave slope would be $k_0 A_0 \simeq 0{\cdot}387$ for $k_0 h \sim \infty$, which is near breaking.

From these figures we note that, for $K = 0$, the wave crests are rather straight except very near the wedge. The picture for the nonlinear cases becomes dramatically different. Here the waves are in general smaller (decreasing for larger K), and the equal phase lines are noticeably bent forward to somewhat beyond 90° along the wedge, forming stems with near-horizontal crest lines. The width of these stems grows linearly with distance so that they all remain inside another wedge whose apex angle increases

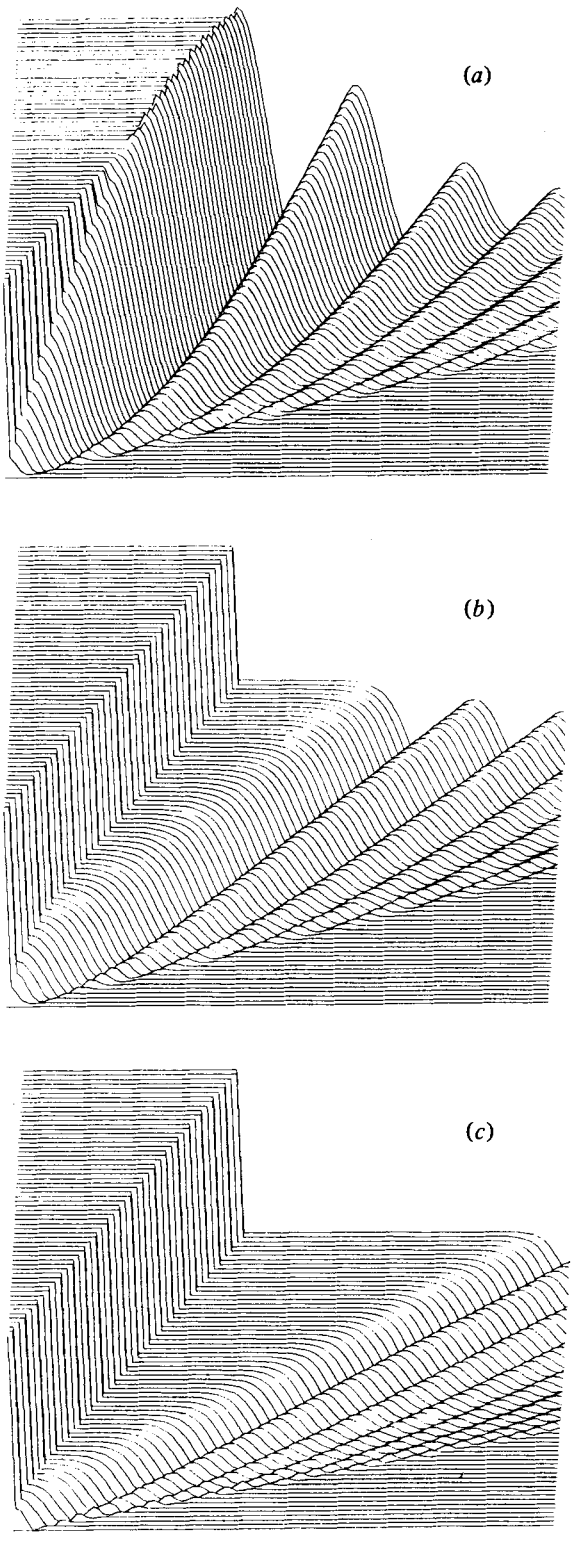

FIGURE 3. Three-dimensional plots of $|\bar{A}(\bar{X}, \bar{Y})|^2$ in the region $0 \leqslant \bar{X} \leqslant 6$, $\bar{X} \leqslant \bar{Y} \leqslant 15$, for (a) $K = 0$, (b) $K = 2$, and (c) $K = 6$. All vertical scales are the same. The wedge is given a height of 5.

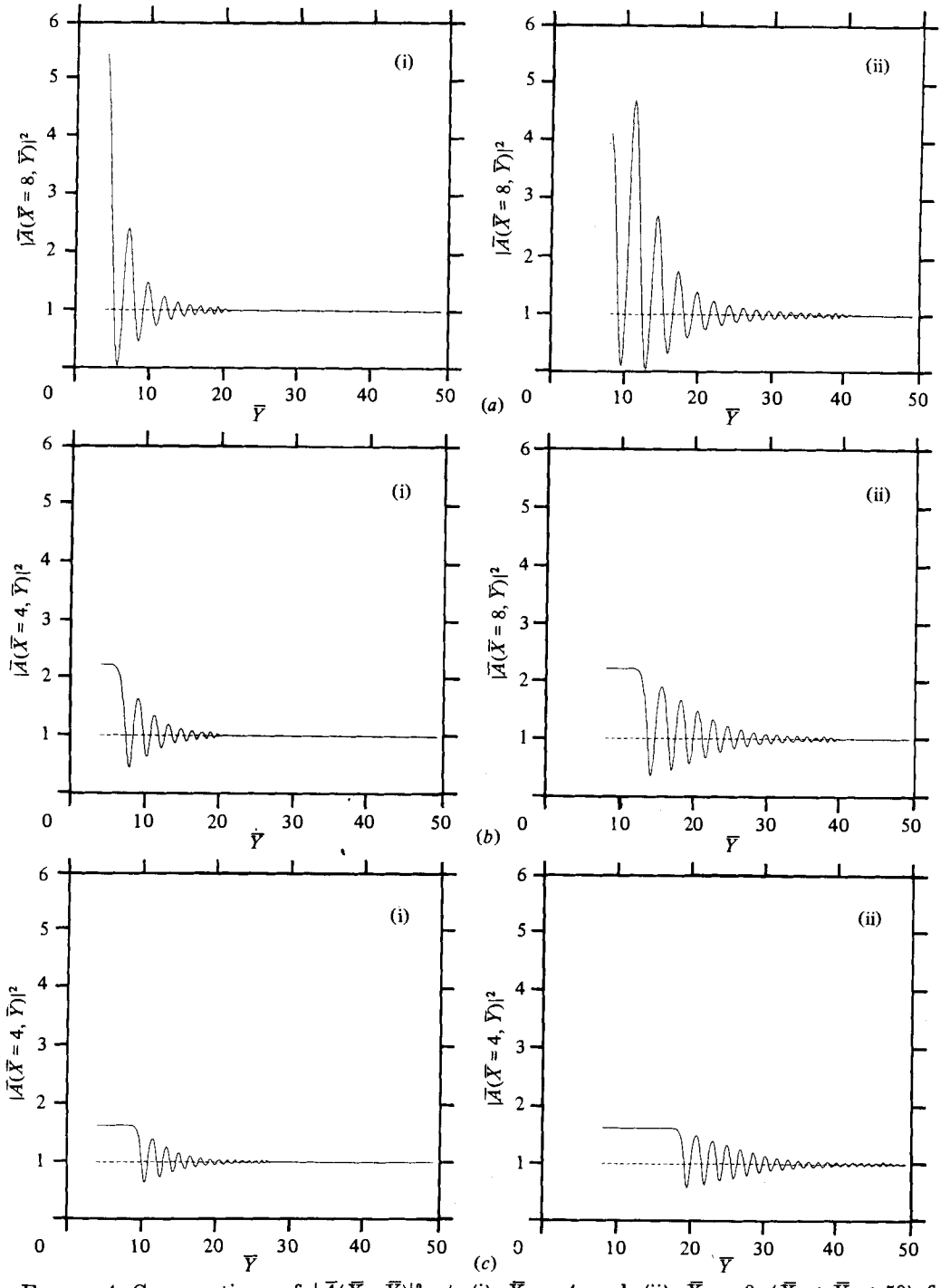

FIGURE 4. Cross-sections of $|\bar{A}(\bar{X}_i, \bar{Y})|^2$ at (i) $\bar{X}_i = 4$ and (ii) $\bar{X}_i = 8$ ($\bar{X} \leqslant \bar{Y} \leqslant 50$) for (*a*) $K = 0$, (*b*) $K = 2$, and (*c*) $K = 6$. (Note that the curves start at the wall of the wedge given by $\bar{Y} = \bar{X}_i$.)

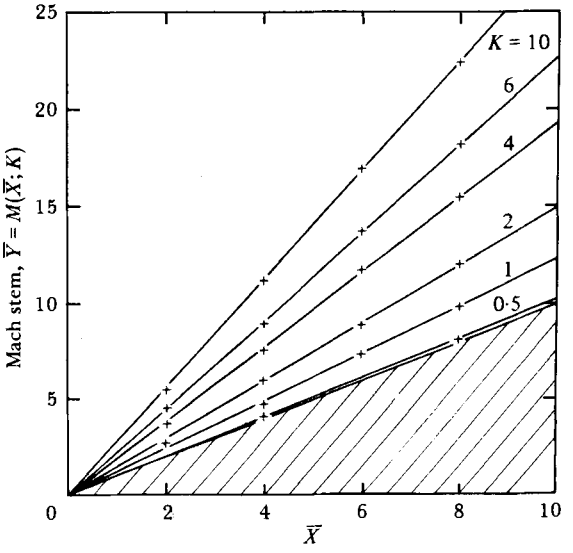

FIGURE 5. Width of the Mach stem region $M(\bar{X}; K)$. +, the edge of the flat region; ——, linear best fit by least square.

with K (and ϵ^2). By comparing the slope of these regions with those found earlier in figure 5, the correspondence is evident, and clearly they also define the boundary of the *Mach stems*. We have thus shown that the numerical–empirical formula (3.7) for M governs the width and rate of growth of the Mach stems. Indeed, if we interpret the change of wavelength, incidence angle, water depth and incident wave height in terms of K, the qualitative conclusions of Nielsen (1962) and Berger & Kohlhase (1976) for the stem width are again confirmed by (3.7) and figure 7. In particular, for those experiments with fixed A_0/h and varying wavelengths, K increases as $(k_0 h)^{-2}$ for small $k_0 h$; thus the slope β can increase with wavelength, as mentioned in the introduction.

4. Approximating the Mach-stem phenomenon by a shock

The computed features associated with the Mach stems are so systematic that some analytical examinations are called for. The sharp bending of wave crests and the near-horizontal plateau of $|\bar{A}|^2$ inside a triangular stem region suggest that the region may be modelled as one side of a straight shock joining two discontinuous constant states. The undulatory variations outside clearly cannot be characterized as a constant region. Nevertheless let us ignore these undulations and examine whether a simple shock model will be able to predict the region of Mach stems. First, we rewrite (3.2a) by letting

$$\bar{A} = a e^{i\psi}, \tag{4.1}$$

where a, ψ are real. Substituting (4.1) into (3.2a) and equating real and imaginary terms respectively, we obtain

$$2a_{\bar{X}} + 2a_{\bar{Y}}\psi_{\bar{Y}} + a\psi_{\bar{Y}\bar{Y}} = 0 \tag{4.2}$$

and

$$2a\psi_{\bar{X}} - a_{\bar{Y}\bar{Y}} + a\psi^2_{\bar{Y}} + Ka^3 = 0, \tag{4.3}$$

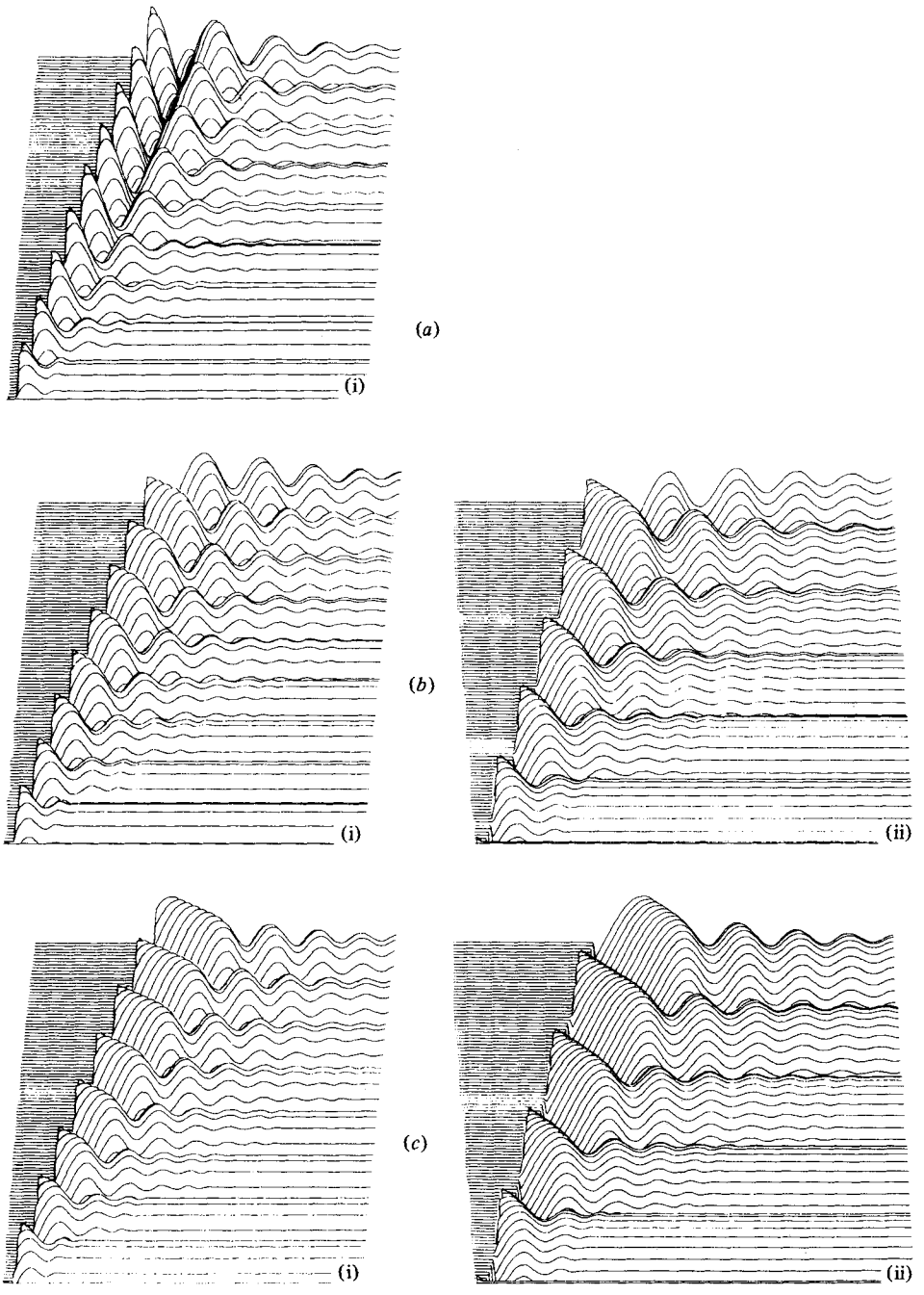

FIGURE 6. Three-dimensional plots of $\zeta_1(k_0 x, k_0 y, t = 0)$ for (i) $\epsilon^2 = 0{\cdot}1$ ($\alpha \simeq 17{\cdot}55°$) and (ii) $\epsilon^2 = 0{\cdot}15$ ($\alpha \simeq 21{\cdot}17°$); and for (*a*) $K = 0$, (*b*) $K = 1$, (*c*) $K = 2$ in uniformly scaled $k_0 x$, $k_0 y$ co-ordinates. The region shown is for $0 \leqslant \bar{X} \leqslant 6$, $\bar{X} \leqslant \bar{Y} \leqslant 18$ corresponding to $0 \leqslant k_0 x \leqslant (60, 40)$, $k_0 x \leqslant k_0 y \leqslant (56{\cdot}92, 46{\cdot}48)$ for $\epsilon^2 = (0{\cdot}1, 0{\cdot}15)$. All vertical scales are the same and the body is given a height of 0.

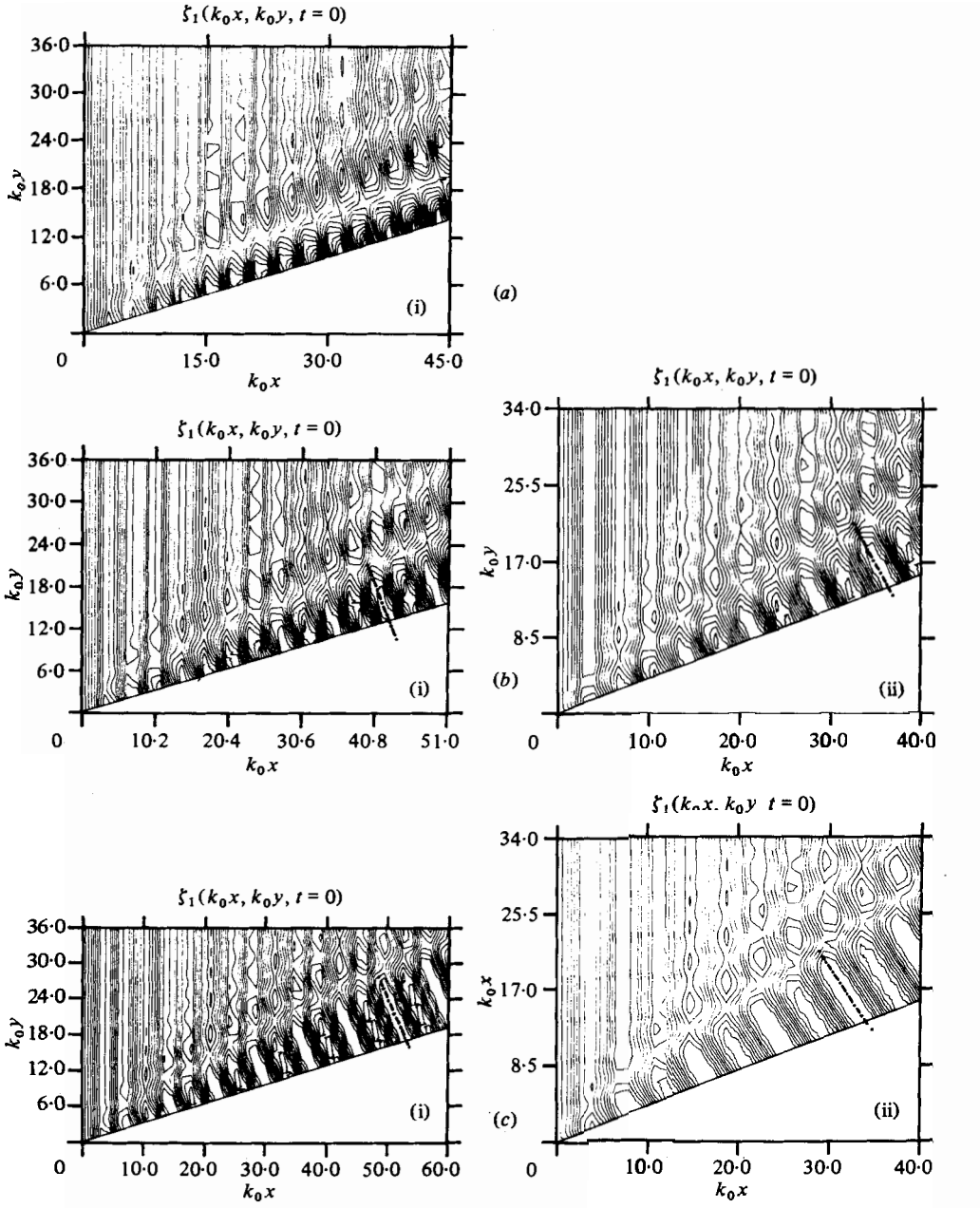

FIGURE 7. Contour plots of $\zeta_1(k_0 x, k_0 y, t = 0)$ for (i) $\epsilon^2 = 0{\cdot}1$ ($\alpha \simeq 17{\cdot}55°$), and (ii) $\epsilon^2 = 0{\cdot}15$ ($\alpha \simeq 21{\cdot}17°$); and for (*a*) $K = 0$, (*b*) $K = 1$, (*c*) $K = 2$ in uniformly scaled $k_0 x$, $k_0 y$ co-ordinates. The contour increment is 0·2. The direction of –·–·– is defined by (4.28).

which can be manipulated to give the conservation equations

$$E_{\bar{X}} + (EW)_{\bar{Y}} = 0 \tag{4.4}$$

and

$$W_{\bar{X}} + \frac{\partial}{\partial \bar{Y}}\left[-\frac{a_{\bar{Y}\bar{Y}}}{2a} + \frac{W^2}{2} + \frac{KE}{2}\right] = 0, \tag{4.5}$$

where

$$E \equiv a^2, \quad W \equiv \psi_{\bar{Y}}. \tag{4.6), (4.7}$$

Equations (4.4) and (4.5) resemble the conservation equations of Chu & Mei (1970) for time-evolving Stokes waves where it is known that omission of the term $a_{\bar{Y}\bar{Y}}$ leads to shocks (Whitham 1967). The transformation between (3.2a) and (4.4)–(4.5) is essentially the same as Davey (1972).

We now ignore $a_{\bar{Y}\bar{Y}}$ and assume that there is a line of discontinuity along $\bar{Y} = \beta\bar{X}$, and that E, W have constant values on either side of this line. It is well known that for a conservation equation

$$\frac{\partial P}{\partial \bar{X}} + \frac{\partial Q}{\partial \bar{Y}} = 0 \tag{4.8}$$

the shock condition is

$$\beta[P] = [Q], \tag{4.9}$$

where

$$[P] = P_+ - P_-, \quad [Q] = Q_+ - Q_- \tag{4.10a,b}$$

and

$$P_\pm \equiv P(\bar{Y} \gtrless \beta\bar{X}), \quad \text{etc.} \tag{4.10c}$$

Thus from (4.4) and (4.5) (neglecting the $a_{\bar{Y}\bar{Y}}$ term) we have

$$\beta(E_+ - E_-) = E_+ W_+ - E_- W_-, \tag{4.11}$$

$$\beta(W_+ - W_-) = \tfrac{1}{2}(W_+^2 - W_-^2) + \tfrac{1}{2}K(E_+ - E_-). \tag{4.12}$$

We now use the known asymptotic values

$$E_+ = E(\bar{Y} \sim +\infty) = 1, \tag{4.13}$$

$$W_+ = \psi_{\bar{Y}}(\bar{Y} \sim +\infty) = 0. \tag{4.14}$$

Furthermore on the wall the boundary condition

$$\frac{\partial \bar{A}}{\partial \bar{Y}} = i\bar{A} \quad \text{on} \quad \bar{Y} = \bar{X} \tag{4.15}$$

implies that

$$W = \psi_{\bar{Y}} = 1 \quad \text{on} \quad \bar{Y} = \bar{X}. \tag{4.16}$$

Consistent with the shock assumption we take

$$W_- = 1 \quad \text{for} \quad \bar{X} < \bar{Y} < \beta\bar{X}. \tag{4.17}$$

Entering (4.13), (4.14) and (4.17) in (4.11) and (4.12), we obtain

$$\beta(1 - E_-) = -E_-, \tag{4.18}$$

$$-\beta = -\tfrac{1}{2} + \frac{K}{2}(1 - E_-). \tag{4.19}$$

It follows after eliminating β that

$$E_- = \frac{1}{2K}[2K + 1 + (8K+1)^{\frac{1}{2}}], \tag{4.20}$$

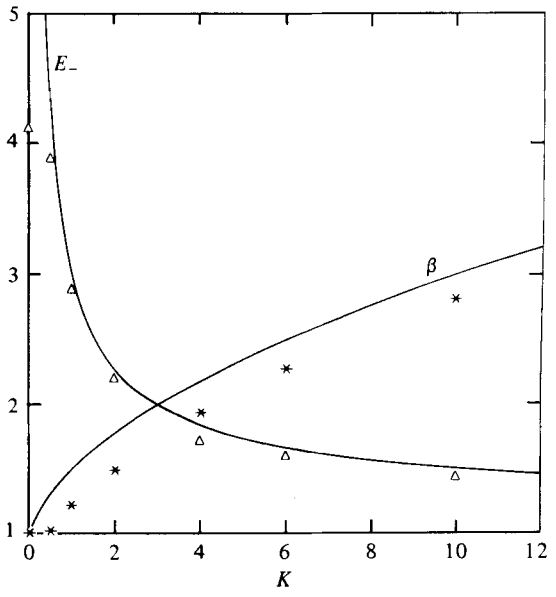

FIGURE 8. Comparison of numerical values for the slope of the Mach-stem region $\beta(K)$ ($\star$) and the amplitude squared along the wall $E_-(K)$ ($\triangle$) with that predicted by shock theory (——).

where the positive sign has been chosen for the radical so that E_- is always positive. The shock slope is then

$$\beta = \frac{E_-}{E_- - 1} = \tfrac{1}{4}[3 + (8K+1)^{\frac{1}{2}}], \tag{4.21}$$

using (4.20). Knowing K from the characteristics of the incident waves and the wedge angle, the squared amplitude inside the Mach-stem region as well as the slope of the stem boundary are thus given theoretically by (4.20) and (4.21). These are compared with the results from the numerical experiments in figure 8. The agreement is surprisingly good, despite the gross simplification of the diffraction region outside the Mach stems.

Finally, let us derive theoretically the angle of bending of the free surface crests across the shock. Integrating (4.17) with respect to Y, we get

$$\psi_- = \bar{Y} + f(\bar{X}), \quad \beta\bar{X} > \bar{Y} > \bar{X}. \tag{4.22}$$

On $\bar{Y} = \beta\bar{X}$, we require $\psi_- = \psi_+$ so that

$$\psi_-|_{\bar{Y}=\beta\bar{X}} = \beta\bar{X} + f(\bar{X}) = \psi_+|_{\bar{Y}=\beta\bar{X}} = \psi|_{\bar{Y}\to\infty} = -\tfrac{1}{2}K\bar{X}, \tag{4.23}$$

using the boundary condition. Hence,

$$f(\bar{X}) = -\tfrac{1}{2}K\bar{X} - \beta\bar{X}. \tag{4.24}$$

Now the free surface displacement is

$$\zeta_1(k_0 x, k_0 y) = \mathrm{Re}\,(\bar{A}\, e^{ik_0 x}) = a\cos(\psi + k_0 x), \tag{4.25}$$

so that

$$\zeta_- = a_- \cos[(k_0 x)(1 - \tfrac{1}{2}\epsilon^2 K - \epsilon^2\beta) + \epsilon(k_0 y)]. \tag{4.26}$$

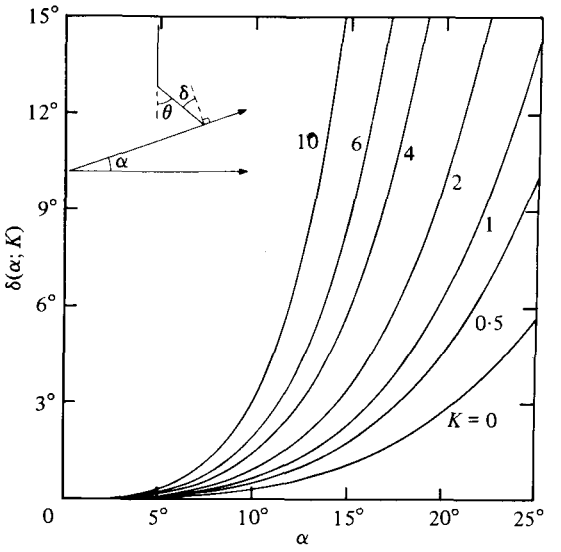

FIGURE 9. Plot of $\delta(\alpha; K)$, the forward inclination of the Mach stems relative to the normal, as predicted by shock theory.

If we denote by θ the angle through which the crests bend across the shock, we have

$$\tan\theta = \frac{\epsilon}{1-\epsilon^2\left[\frac{K}{2}+\beta\right]} = \frac{\epsilon}{1-\epsilon^2\left[\frac{K}{2}+\frac{3+(8K+1)^{\frac{1}{2}}}{4}\right]} > \epsilon \tag{4.27}$$

on using (4.21) for β.

To the leading order $\tan\theta \simeq \epsilon \equiv \tan\alpha$, so that the Mach stems are approximately orthogonal to the wall. To assess the small effect of K, we define the angle away from the normal by $\delta = \theta - \alpha$, then

$$\tan\delta = \tan(\theta-\alpha) = \frac{\epsilon^3\left[\frac{K}{2}+\frac{3+(8K+1)^{\frac{1}{2}}}{4}\right]}{1-\epsilon^2\left[\frac{K}{2}+\frac{(8K+1)^{\frac{1}{2}}-1}{4}\right]}, \tag{4.28}$$

which is an $O(\epsilon)^3$ quantity; δ is plotted as a function of α and K in figure 9. To compare with computed results, the directions of the stem given by (4.28) are added as broken lines (·–·–·) in the contours of ζ_1 in figure 7. The agreement is again satisfactory.

Despite these agreements, it should be stressed that other conservation equations may be derived from (4.4) and (4.5), implying that a different pair of shock conditions may be used. Whether the present pair is the most appropriate is by no means clear. Because of the recognized shortcomings on one side of the shock, this ambiguity does not seem worth pursuing any further.

We are grateful for the support by the Fluid Mechanics programs of the U.S. National Science Foundation (ENG 77-17817), and of the U.S. Office of Naval Research (NR 062-228).

Appendix. Outline of derivation of the approximate equations

Substituting (2.14)–(2.16) into (2.3) and expanding in Taylor series about $z = 0$, we obtain a sequence of perturbation problems

$$\left(\frac{\partial^2}{\partial x^2}+\frac{\partial^2}{\partial z^2}\right)\phi_n = F_n \quad \text{for} \quad -h < z < 0, \tag{A 1}$$

$$\left(g\frac{\partial}{\partial z}+\frac{\partial^2}{\partial t^2}\right)\phi_n = G_n \quad \text{on} \quad z = 0, \tag{A 2}$$

$$\frac{\partial \phi_n}{\partial z} = 0 \quad \text{on} \quad z = -h \tag{A 3}$$

and

$$-g\zeta_n = H_n \quad \text{on} \quad z = 0, \tag{A 4}$$

where F_n, G_n, H_n are given by lower-order terms. Finally, we introduce the Fourier expansions

$$(\phi_n, F_n, \zeta_n, G_n, H_n) = \sum_{m=-n}^{n} e^{im\psi}(\phi_{mn}, F_{mn}, \zeta_{mn}, G_{mn}, H_{mn}), \tag{A 5}$$

where $(\ )_{-m,n}$, $(\ )_{m,n}$ are complex conjugates so that the variables on the left-hand side remain real, and

$$\psi = k_0 x - \omega t, \tag{A 6}$$

$$\omega^2 = k_0 g \tanh k_0 h. \tag{A 7}$$

Note that ϕ_{mn}, F_{mn} are now complex functions of (X, Y, z), and ζ_{mn}, G_{mn}, H_{mn} that of X, Y) only. If we substitute (A 5) into (A 1)–(A 3) and use (A 4), we obtain at each m and n a boundary-value problem in z:

$$\left(\frac{\partial^2}{\partial z^2}-m^2k_0^2\right)\phi_{mn} = F_{mn} \quad \text{for} \quad -h < z < 0, \tag{A 8a}$$

$$\left(g\frac{\partial}{\partial z}-m^2\omega^2\right)\phi_{mn} = G_{mn} \quad \text{on} \quad z = 0, \tag{A 8b}$$

$$\frac{\partial}{\partial z}\phi_{mn} = 0 \quad \text{on} \quad z = -h. \tag{A 8c}$$

At any n, non-trivial homogeneous solutions to the above boundary-value problem will only exist for $m = 0$ and $m = \pm 1$, in which case F_{mn} and G_{mn} must satisfy solvability conditions to avoid secularity. In particular we require

$$\frac{1}{g}G_{0n} = \int_{-h}^{0} F_{0n}\,dz \quad \text{for} \quad m = 0 \tag{A 9}$$

and

$$\frac{1}{g}G_{mn} = \int_{-h}^{0} F_{mn}\frac{\cosh k_0(z+h)}{\cosh k_0 h}\,dz \quad \text{for} \quad m = \pm 1. \tag{A 10}$$

The wave field to second order is found to be

$$\phi = \epsilon\left[\phi_{01} - \frac{g\cosh Q}{2\omega\cosh q}(iA\,e^{i\psi} + *)\right] + \epsilon^2\left[\phi_{02} - \frac{g\cosh Q}{2\omega\cosh q}(iB\,e^{i\psi} + *) - \frac{3\omega\cosh 2Q}{16\sinh^4 q}(iA^2 e^{2i\psi} + *)\right], \quad \text{(A 11)}\dagger$$

$$\zeta = \epsilon[\tfrac{1}{2}(A\,e^{i\psi} + *)] + \epsilon^2\left[\tfrac{1}{2}(B\,e^{i\psi} + *) - \frac{k_0}{2\sinh 2q}|A|^2 + \frac{k_0\cosh q\,(2\cosh^2 q + 1)}{8\sinh^3 q}(A^2 e^{2i\psi} + *)\right], \quad \text{(A 12)}\dagger$$

where $*$ denotes the complex conjugate of the preceding term,

$$Q = k_0(z+h), \quad q = k_0 h \qquad \text{(A 13)}$$

and ϕ_{01}, ϕ_{02}, A, B are complex functions of the slow variables (X, Y) only. In particular, at third order, solvability condition (A 10) gives equation (2.17), after simplification.

REFERENCES

Benjamin, T. B. & Feir, J. E. 1967 The disintegration of wave trains on deep water. Part 1. Theory. *J. Fluid Mech.* **27**, 417–430.

Berger, U. & Kohlhase, S. 1976 Mach reflection as a diffraction problem. *Proc. 15th Conf. Coastal Engng.*

Benney, D. J. & Roskes, G. J. 1969 Wave instabilities. *Stud. Appl. Math.* **48**, 377–385.

Chakrabarti, S. K. 1978 Comments on second-order wave effects on large diameter vertical cylinder. *J. Ship. Res.* **22**, 266–268.

Chen, T. C. 1961 Experimental study on the solitary wave reflection along a straight sloped wall at oblique angle of incidence. *U.S. Beach Erosion Board Tech. Memo.* 124.

Chu, V. H. & Mei, C. C. 1970 On slowly varying Stokes waves. *J. Fluid Mech.* **41**, 873–887.

Davey, A. 1972 The propagation of a weak nonlinear wave. *J. Fluid Mech.* **53**, 769–781.

Davey, A. & Stewartson, K. 1974 On three-dimensional packets of surface waves. *Proc. Roy. Soc.* A **338**, 101–110.

Fock, V. A. 1946 The field of a plane wave near the surface of a conducting body. *J. Phys. U.S.S.R.* **10**, 399–409.

Fock, V. A. 1960 *Electromagnetic Diffraction and Propagation Problems.* New York: Macmillan.

Isaacson, M. St Q. 1977 Nonlinear wave forces on large offshore structures. *J. Waterways, Port, Coastal and Ocean Div., A.S.C.E.* **101**, 166–170.

Karpman, V. I. 1975 *Nonlinear Waves in Dispersive Media.* Pergamon.

Lee, C. M. 1966 The second-order theory of cylinders oscillating vertically in a free surface. Dissertation, University of California, Berkeley.

Leontovich, M. A. 1944 A method of solution of problems of electromagnetic wave propagation along the earth's surface. *Izv. Akad. Nauk S.S.S.R.* **8**, 16–22 (in Russian).

Lighthill, M. J. 1949 The diffraction of blast. I. *Proc. Roy. Soc.* A **198**, 454–470.

Mei, C. C. & Tuck, E. O. 1980 Forward scattering by long thin bodies. *SIAM J. Appl. Math.* (to appear).

Miles, J. W. 1977*a* Resonantly interacting solitary waves. *J. Fluid Mech.* **79**, 171–179.

† By carrying out the perturbation analysis to the fourth order, it can be shown that both ϕ_{01} and B will vanish (assuming that they are absent in the incident wave) and, in fact, A determines the entire wave field to $O(\epsilon^2)$.

MILES, J. W. 1977*b* Diffraction of solitary waves. *Z. angew. Math. Phys.* **28**, 889–902.

MOLIN, B. 1979 Second-order diffraction loads upon three-dimensional bodies. *Appl. Ocean Res.* (to appear).

NIELSEN, A. H. 1962 Diffraction of periodic waves along a vertical breakwater for small angles of incidence. *Univ. of California, Berkeley, IER Tech. Rep.* HEL-1-2.

PERROUD, P. H. 1957 The solitary wave reflection along a straight vertical wall at oblique incidence. *Univ. of California, Berkeley, IER Tech. Rep.* 99-3.

RAMAN, J., JOTHISHANKAR, N. & VENKATANARASAIAH, P. 1977 Nonlinear wave interaction with vertical cylinders of large diameter. *J. Ship Res.* **21**, 120–124.

TAPPERT, F. 1977 The parabolic approximation method. In *Wave Propagation and Underwater Acoustics* (ed. J. B. Keller & J. S. Papadakis), Lecture notes in Physics, vol. 70, pp. 224–287. Springer.

WHITHAM, G. B. 1967 Variational methods and applications to water waves. *Proc. Roy. Soc.* A **299**, 6–25.

WHITHAM, G. B. 1974 *Linear and Nonlinear Waves.* Wiley-Interscience.

WIEGEL, R. L. 1964*a* *Oceanographical Engineering.* Prentice-Hall.

WIEGEL, R. L. 1964*b* Water wave equivalent of Mach-reflection. *Proc. 9th Conf. Coastal Engng A.S.C.E.*, vol. 6, pp. 82–102.

ZAKHAROV, V. E. & SHABAT, A. B. 1972 Exact theory of two-dimensional self-focusing and one-dimensional self-modulation of waves in nonlinear media. *Sov. Phys., J. Exp. Theor. Phys.* **34**, 62–69.